


# Effects of viscosity and scission configuration on the fission dynamics of the excited compound nucleus $^{240}\text{Pu}$ produced in neutron-induced reactions

H. Eslamizadeh <sup>\*</sup>*Department of Physics, Faculty of Nano and Bio Science and Technology, Persian Gulf University, 75169 Bushehr, Iran*

(Received 24 August 2023; revised 4 November 2023; accepted 5 January 2024; published 5 February 2024)

The fission process of the excited compound nucleus  $^{240}\text{Pu}$  produced in neutron-induced reactions at incident energies from thermal to 14 MeV has been simulated by using a stochastic approach based on four-dimensional Langevin equations. The fission cross section, the total kinetic energy of fission fragments, the mass distribution of fission fragments, the average prompt neutron multiplicity, the average spin of fission fragments, and the mean fission time have been calculated for the excited compound nucleus  $^{240}\text{Pu}$ . Three collective shape coordinates plus the projection of total spin of the compound nucleus on the symmetry axis,  $K$ , were considered in the four-dimensional dynamical model. In the dynamical calculations the effect of the neck radius in the scission configuration on the total kinetic energy of fission fragments of the  $^{240}\text{Pu}$  nucleus was examined. In the dynamical calculations, nuclear dissipation was generated through the chaos weighted wall-and-window friction formula with a chaoticity coefficient  $\mu$ . In the calculations, the chaoticity coefficient was considered as a free parameter and its magnitude was inferred for  $^{240}\text{Pu}$  by fitting measured data on the fission cross section. It was shown that the results of calculations for the fission cross section are in good agreement with the experimental data by using the magnitude of the chaoticity coefficient  $\mu = 0.4$ . Furthermore, by reproducing experimental data on the total kinetic energy of fission fragments for the excited compound nucleus  $^{240}\text{Pu}$ , the magnitude of the neck radius at which rupture occurs was inferred. It was shown that the results of the total kinetic energy of fission fragments are very sensitive to the value of the neck radius at which rupture occurs. It was also shown that the results of calculations for the total kinetic energy of fission fragments for  $^{240}\text{Pu}$  are in good agreement with the experimental data by using the magnitude of the radius in the scission configuration equal to 2.2 fm. Furthermore, the mass distribution of fission fragments and the average prompt neutron multiplicity have also been calculated for  $^{240}\text{Pu}$  by using these appropriate values for the chaoticity coefficient and the neck radius in the scission configuration. Comparison of the calculated data with the experimental data has shown that the results of calculations are in good agreement with the experimental data by using these appropriate values. Finally, the average spin of fission fragments and the mean fission time have also been calculated for  $^{240}\text{Pu}$ . It was shown that the average spin of fission fragments is strongly mass dependent and has a sawtooth shape, and also the mean fission time decreases rapidly with increasing incident neutron energy.

DOI: [10.1103/PhysRevC.109.024602](https://doi.org/10.1103/PhysRevC.109.024602)

## I. INTRODUCTION

Although the phenomenon of nuclear fission was discovered 80 years ago, the study of fission is still of general interest. Furthermore, the dynamical process towards the scission point is still not completely understood, and knowledge about the scission configuration is quite lacking. Also, a comprehensive model has not yet been presented for a description of this process. Fission may take place in any of the heavy nuclei after capture of a neutron. However, thermal neutrons are able to cause fission only in some isotopes of transuranic elements whose nuclei contain odd numbers of neutrons, for example  $^{233}\text{U}$ ,  $^{235}\text{U}$ , and  $^{239}\text{Pu}$ . For nuclei containing an even number of neutrons, fission can only occur if the incident neutrons have energy above about  $10^6$  eV. After a fission event, fission fragments generally are highly excited, and they

deexcite by emitting several light particles such as prompt neutrons,  $\gamma$  rays, and delayed neutrons. It should be mentioned that fission fragments yield plays an important role in many nuclear physics applications such as radioisotope production for medical applications, development of advanced reactors, and so on. The nuclear fission of nuclei can be described by statistical or dynamical models (see for example Refs. [1–15]). The Langevin equations or the Fokker-Planck equation generally have been used in the dynamical calculations. However, during the last three decades the Langevin equations has been used extensively to describe fission of excited compound nuclei. The Fokker-Planck equation can be solved only by using approximate methods, while numerical solution of the Langevin equations is possible nearly without any approximations. It should be noted that in simulation of the fission process of a compound nucleus it is very important to consider the evolution of the projection of total spin of the compound nucleus on the symmetry axis [16,17]. In the present research, the four-dimensional (4D) dynamical model

---

\*eslamizadeh@pgu.ac.ir

based on the Langevin equations is used to simulate the fission process of the excited compound nucleus  $^{240}\text{Pu}$  produced in the  $n + ^{239}\text{Pu}$  reaction at incident energies from thermal to 14 MeV. The fission cross section, the total kinetic energy of fission fragments, the mass distribution of fission fragments, the average prompt neutron multiplicity, the average spin of fission fragments, and the mean fission time are calculated for  $^{240}\text{Pu}$ . It should be stressed that at low excitation energy it is essential to consider quantum (shell and pairing) effects. For example, consideration of the shell effects causes production of a double-humped shape of the mass and charge distributions of fission fragments. By excluding shell effects, one will often obtain only a single-humped result. In the calculations, the shell effects can be considered in calculation of the potential energy surface.

The main motivation of this work is to investigate the effects of the neck radius in the scission configuration and the nuclear dissipation on the fission process of  $^{240}\text{Pu}$ .

The present paper has been arranged as follows: the model and basic equations are described in Sec. II. The results of calculations are presented in Sec. III. Finally, the concluding remarks are given in Sec. IV.

## II. DETAILS OF THE MODEL AND BASIC EQUATIONS

In the present research, a dynamical model based on the 4D dynamical model is used to simulate the fission process of  $^{240}\text{Pu}$  nucleus produced in  $n + ^{239}\text{Pu}$  reaction. Three collective shape coordinates plus the projection of total spin of the compound nucleus to the symmetry axis,  $K$ , are considered in the 4D dynamical model. In the 4D dynamical model, the time evolution of an excited compound nucleus can be considered by the coupled Langevin equations. The Langevin equations can be defined as a system of first-order differential equations as follows:

$$\begin{aligned} \dot{q}_i &= \mu_{ij} p_j, \\ \dot{p}_i &= -\frac{1}{2} p_j p_k \frac{\partial \mu_{jk}}{\partial q_i} - \frac{\partial F}{\partial q_i} - \gamma_{ij} \mu_{jk} p_k + \theta_{ij} \xi_j, \end{aligned} \quad (1)$$

in these equations summation is assumed over repeated indices. In Eq. (1)  $\mathbf{q} = (q_1, q_2, q_3)$  are the collective coordinates and  $\mathbf{p} = (p_1, p_2, p_3)$  are the momenta conjugate to them. The driving potential is given by the Helmholtz free energy  $F(\mathbf{q}, K) = V(\mathbf{q}, K) - a(\mathbf{q})T^2$ , where  $V(\mathbf{q}, K)$  is the potential energy. The deformation dependence of the level density parameter can be determined as [18]

$$a(\mathbf{q}) = a_v A + a_s A^{2/3} B_s(\mathbf{q}), \quad (2)$$

where  $B_s$  is the dimensionless functional of the surface energy in the liquid-drop model and  $A$  is the mass number of the fissile nucleus. The coefficients  $a_v = 0.073 \text{ MeV}^{-1}$  and  $a_s = 0.095 \text{ MeV}^{-1}$  are taken from Ref. [18]. In Eq. (1)  $\gamma_{ij}$  is the friction tensor,  $m_{ij} (\|\mu_{ij}\| = \|m_{ij}\|^{-1})$  is the tensor of inertia,  $\theta_{ij} \xi_j$  is a random force,  $\theta_{ij}$  is its amplitude, and  $\xi_j(t)$  is a random variable that possesses the following statistical properties  $\langle \xi_i \rangle = 0$  and  $\langle \xi_i(t_1) \xi_j(t_2) \rangle = 2\delta_{ij} \delta(t_1 - t_2)$ .

In the present research the two-center shell model shape parametrization (TCSM) [19] is used as the collective shape

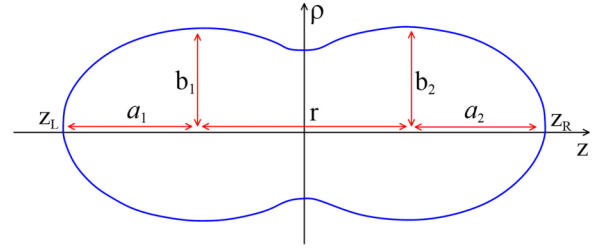


FIG. 1. Shape parametrizations based on the TCSM for a fissioning system.

coordinates. In terms of this parametrization one can describe both compact shapes and separated fragments. In the TCSM parametrization, the collective coordinates are  $(q_1, q_2, q_3) = (r/R_0, \eta, \alpha)$ , where  $r$  is the distance between the centers of the nascent fragments,  $R_0$  is the radius of the spherical compound nucleus, and  $\alpha = (A_1 - A_2)/(A_1 + A_2)$  is the mass asymmetry of the two fragments, where  $A_1$  and  $A_2$  are the mass numbers of fragments. The parameter  $\eta$  is the deformation of the fragments, and can be defined as  $\eta_i = 3(a_i - b_i)/(2a_i + b_i)$  with  $i = 1, 2$  for each fragment. Parameters  $a_i$  and  $b_i$  are the half lengths of the axes of an ellipse in  $z$  and  $\rho$  directions of the cylindrical coordinates, as shown in Fig. 1.

It should be mentioned that, in the present research, it is assumed that the shapes of the fission fragment tips of the left and right fragments are the same ( $\eta = \eta_1 = \eta_2$ ).

In the present calculations, the simulation of the fission process of the compound nucleus is considered from the ground state with the excitation energy  $E^*$ . The initial conditions can be generated by the Neumann method with the generating function

$$\begin{aligned} P(\mathbf{q}_0, \mathbf{p}_0, I, t = 0) &\approx \exp\left[-\frac{V(\mathbf{q}_0, I, K) + E_{\text{coll}}(\mathbf{q}_0, \mathbf{p}_0)}{T}\right] \\ &\times \delta(\mathbf{q}_0 - \mathbf{q}_{gs}) \frac{d\sigma(I)}{dI}, \end{aligned} \quad (3)$$

where  $\mathbf{q}_{gs}$  are the coordinates of the ground state of the compound nucleus. The initial shape of the nucleus is assumed to be spherical,  $\mathbf{q}_0 = \mathbf{q}_{gs} = (r/R_0 = 0.75, \eta = 0.0, \alpha = 0.0)$ , and the momentum distribution is taken to be in equilibrium. The initial spin for each Langevin trajectory can be sampled by the Monte Carlo method from the following spin distribution [20]:

$$\frac{d\sigma(I)}{dI} = \frac{2\pi}{k^2} \frac{2I + 1}{1 + \exp\left(\frac{I - I_c}{\delta I}\right)}, \quad (4)$$

where  $\delta I$  is the diffuseness and  $I_c$  is the critical spin. The parameters  $\delta I$  and  $I_c$  can be approximated by the relations presented in Ref. [20]. Figure 2 shows the spin distribution for  $^{240}\text{Pu}$  as a function of spin produced in the  $n + ^{239}\text{Pu}$  reaction, for example, for projectile energies  $E_{\text{c.m.}} = 5, 7, 10 \text{ MeV}$ . It is clear from Fig. 2 that, with increasing projectile energy, the probability of forming the compound nucleus with higher spin increases.

It should be mentioned that many authors in their calculations describing different features of the fission process of excited nuclei assumed that the nuclei have zero spin about

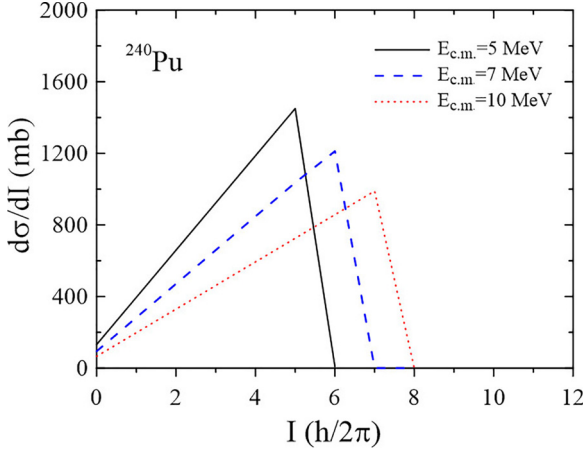


FIG. 2. The spin distribution for  $^{240}\text{Pu}$  as a function of spin for projectile energies  $E_{c.m.} = 5, 7, 10$  MeV .

the symmetry axis. However, this assumption is incorrect. The authors of Ref. [21] showed that evolution of the  $K$  collective coordinate can be considered as

$$dK = -\frac{\gamma_K^2 I^2}{2} \frac{\partial V}{\partial K} dt + \gamma_K I \xi(t) \sqrt{T} dt, \quad (5)$$

where  $\xi(t)$  has the same properties as in Eq. (1) and  $\gamma_K$  is a parameter controlling the coupling between the orientation degree of freedom  $K$  and the heat bath. The authors of Refs. [17,21] based on the works of Døssing and Randrup [22,23] have shown that  $\gamma_K$  in the case of a dinucleus can be determined as

$$\gamma_K = \frac{1}{R_N r \sqrt{2\pi^3 n_0}} \sqrt{\frac{J_R |J_{\text{eff}}| J_{\parallel}}{J_{\perp}^3}}, \quad (6)$$

where  $J_R = M_0 r^2/4$  for a reflection symmetric shape,  $J_{\parallel}$  and  $J_{\perp}$  are the rigid body moments of inertia about and perpendicular to the symmetry axis, and  $J_{\text{eff}}$  is the effective moment of inertia:  $J_{\text{eff}} = [J_{\parallel}^{-1} - J_{\perp}^{-1}]^{-1}$ . The rigid body moments of inertia, about and perpendicular to the symmetry axis, can be determined as in Ref. [24].  $R_N$  is the neck radius,  $r$  is the distance between the centers of mass of the nascent fragments, and  $n_0 = 0.0263 \text{ MeVzs}^4 \text{ fm}^{-4}$  is the bulk flux in the standard nuclear matter [22]. It should be mentioned that Eq. (5), and the Langevin equations, Eq. (1), are connected through the potential energy. For a dinucleus the magnitude of  $\gamma_K$  can be determined according to Eq. (6). On the other hand, in order to perform numerical integration of the Langevin equation for the  $K$  coordinate one needs to determine the value of  $\gamma_K$  for all possible nuclear deformations. The magnitude of  $\gamma_K$  for mononuclear shapes can be determined by extrapolating Eq. (6). It should be mentioned that Lestone and McCalla in Ref. [25] showed that the  $\gamma_K$  coefficient for compound nuclei with shapes featuring a neck has a small value,  $0.0077 (\text{MeVzs})^{-1/2}$ . Furthermore, Nadochy *et al.* in Ref. [12] used the deformation dependent  $\gamma_k$  in the four-dimensional dynamical Langevin model and showed that, for reproducing experimental data on the anisotropy of the fission fragment angular distribution, the  $\gamma_k$  coefficient

should increase up to  $0.2\text{--}0.4 (\text{MeVzs})^{-1/2}$  for compact shapes featuring no neck for the compound nuclei with  $A_{CN} \cong 200$  and up to  $0.1\text{--}0.2 (\text{MeVzs})^{-1/2}$  for the heavier nuclei with  $A_{CN} \cong 250$ .

For a given value of a temperature of a system, the potential energy at low excitation energy can be calculated on the basis of the finite-range liquid drop model [26,27] considering shell correction as follows:

$$V(\mathbf{q}, I, K, T) = V_{SH}(\mathbf{q}, T) + V_{LDM}(\mathbf{q}) + E_{rot}, \quad (7)$$

where  $V_{SH}(\mathbf{q}, T)$  is the shell correction energy that can be evaluated by the Strutinski method from the single-particle levels of the two-center shell model [28,29]. The shell correction can be given as

$$V_{SH}(\mathbf{q}, T) = E_{\text{shell}}^0(\mathbf{q})\Phi(T), \quad (8)$$

where factor  $\Phi(T)$  is the temperature dependence of the shell correction. Factor  $\Phi(T)$  can be calculated by [30]

$$\Phi(T) = \exp\left(-\frac{aT^2}{E_d}\right), \quad (9)$$

where  $a$  is the level density parameter and  $E_d$  is the shell damping energy. The magnitude of  $E_d = 20 \text{ MeV}$  was suggested by Ignatyuk and his coauthors in Ref. [18]. The shell correction energy at zero temperature reduces to  $E_{\text{shell}}^0$ . The shell correction energy at zero temperature can be determined with the pairing energy and the shell effects in total single-particle energy as follows:

$$E_{\text{shell}}^0(\mathbf{q}, T = 0) = \sum_{n,p} [E_{\text{shell}}^{(n,p)}(\mathbf{q}) + E_{\text{pair}}^{(n,p)}(\mathbf{q})], \quad (10)$$

where  $E_{\text{shell}}^{(n,p)}(\mathbf{q})$  and  $E_{\text{pair}}^{(n,p)}(\mathbf{q})$  can be calculated in the Bardeen-Cooper-Schrieffer (BCS) approximation [29,31] and the Strutinsky prescription [28,31,32].

The rotational part of the potential energy is calculated by

$$E_{rot}(\mathbf{q}, I, K) = \frac{\hbar^2 I(I+1)}{2J_{\perp}(\mathbf{q})} + \frac{\hbar^2 K^2}{2J_{\text{eff}}(\mathbf{q})}. \quad (11)$$

Figure 3 shows the potential energy surface for the compound nucleus  $^{240}\text{Pu}$  as a function of the collective coordinates  $r/R_0$  and  $\alpha$  (for example) at  $\eta = 0.15$ . It should be mentioned that Fig. 3 presents the potential energy surface for the compound nucleus  $^{240}\text{Pu}$  considering a similar small deformation for the fission fragments,  $\eta_1 = \eta_2 = 0.15$ .

In the present calculations, dissipation is generated through the chaos weighted wall-and-window friction formula. For small elongation before neck formation, the chaos weighted wall formula is used to calculate the friction tensor and after neck formation used the chaos weighted wall-and-window friction formula [33],

$$\gamma_{ij} = \begin{cases} \mu(q_1) \gamma_{ij}^{\text{wall}} & \text{for nuclear shapes featuring no neck,} \\ \mu(q_1) \gamma_{ij}^{\text{wall}} + \gamma_{ij}^{\text{win}} & \text{for nuclear shapes featuring a neck.} \end{cases} \quad (12)$$

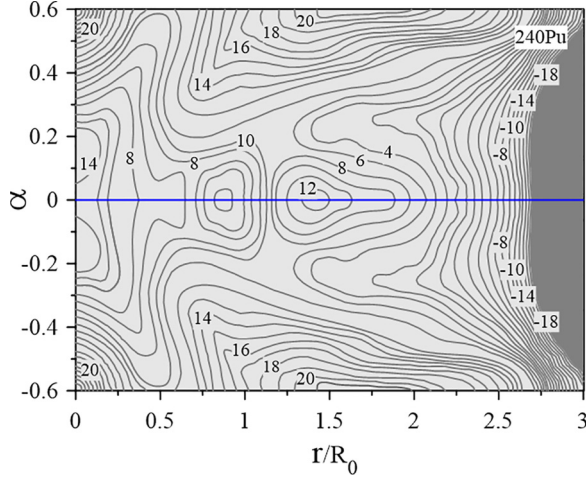


FIG. 3. The potential energy surface as a function of the collective coordinates  $r/R_0$  and  $\alpha$  at  $\eta = 0.15$  for the compound nucleus  $^{240}\text{Pu}$ . The numbers at the contour lines represent the potential energy values in MeV.

The chaoticity  $\mu$  is a measure of chaos in the single-particle motion and depends on the shape of the nucleus. The magnitude of chaoticity  $\mu$  changes from 0 to 1 as the nucleus evolves from spherical to a deformed shape. The magnitude of the chaoticity  $\mu$  can be determined as in Ref. [34]. The value  $\mu = 1$  corresponds to the standard wall and wall-plus-window formulas. It should be mentioned that in the present research for simplicity it is assumed that  $\mu(\mathbf{q}) \cong \mu(q_1)$ . Figure 4 shows the chaoticity  $\mu$  for  $^{240}\text{Pu}$  as a function of  $q_1 = r/R_0$ .

In Eq. (12)  $\gamma_{ij}^{\text{wall}}$  and  $\gamma_{ij}^{\text{win}}$  can be given by the relations presented in Refs. [33,35]. For nuclear shapes featuring no neck

$$\gamma_{ij}^{\text{wall}} = \frac{\pi \rho_m \bar{v}}{2} \int_{z_{\min}}^{z_{\max}} \left( \frac{\partial \rho_s^2}{\partial q_i} \right) \left( \frac{\partial \rho_s^2}{\partial q_j} \right) \left[ \rho_s^2 + \left( \frac{1}{2} \frac{\partial \rho_s^2}{\partial z} \right)^2 \right]^{-1/2} dz, \quad (13)$$

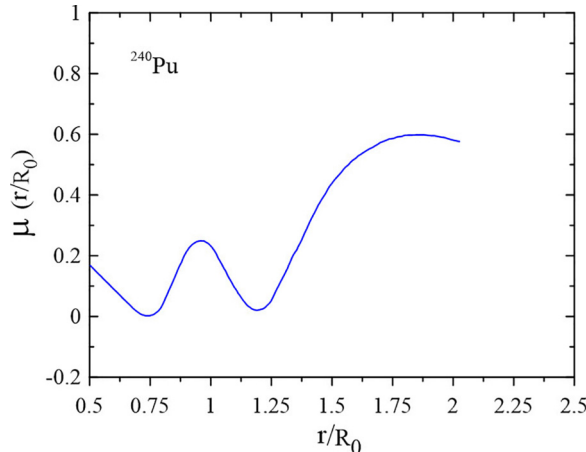


FIG. 4. The magnitude of chaoticity  $\mu$  as a function of  $r/R_0$  for the compound nucleus  $^{240}\text{Pu}$ .

and for nuclear shapes featuring a neck

$$\gamma_{ij}^{\text{wall}} = \frac{\pi \rho_m \bar{v}}{2} \left\{ \int_{z_{\min}}^{z_N} \left( \frac{\partial \rho_s^2}{\partial q_i} + \frac{\partial \rho_s^2}{\partial z} \frac{\partial D_1}{\partial q_i} \right) \times \left( \frac{\partial \rho_s^2}{\partial q_j} + \frac{\partial \rho_s^2}{\partial z} \frac{\partial D_1}{\partial q_j} \right) \left[ \rho_s^2 + \left( \frac{1}{2} \frac{\partial \rho_s^2}{\partial z} \right)^2 \right]^{-1/2} dz + \int_{z_N}^{z_{\max}} \left( \frac{\partial \rho_s^2}{\partial q_i} + \frac{\partial \rho_s^2}{\partial z} \frac{\partial D_2}{\partial q_i} \right) \left( \frac{\partial \rho_s^2}{\partial q_j} + \frac{\partial \rho_s^2}{\partial z} \frac{\partial D_2}{\partial q_j} \right) \times \left[ \rho_s^2 + \left( \frac{1}{2} \frac{\partial \rho_s^2}{\partial z} \right)^2 \right]^{-1/2} dz \right\}, \quad (14)$$

$$\gamma_{ij}^{\text{win}} = \frac{1}{2} \rho_m \bar{v} \left\{ \left( \frac{\partial r}{\partial q_i} \frac{\partial r}{\partial q_j} \right) \Delta \sigma + \frac{32}{9} \frac{1}{\Delta \sigma} \frac{\partial V_1}{\partial q_i} \frac{\partial V_1}{\partial q_j} \right\}, \quad (15)$$

where  $\rho_m$  is the mass density of the nucleus,  $\bar{v}$  is the average nucleon speed inside the nucleus,  $r$  is the distance between centers of mass of future fragments,  $\Delta \sigma$  is the area of the window between two parts of the system,  $V_1$  is the volume of one of the would-be fragments,  $\rho_s$  is the radial coordinate of the nuclear surface,  $D_1$  and  $D_2$  are positions of mass centers of the two parts of the fissioning system relative to the center of mass of the whole system,  $z_{\min}$  and  $z_{\max}$  are the left and right ends of the nuclear shape, and  $z_N$  is the position of the neck plane that divides the nucleus into two parts. In the present calculations the inertia tensor is calculated by the Werner-Wheeler approximation for the incompressible and irrotational flow [36] as

$$m_{ij} = \pi \rho_m \int_{z_{\min}}^{z_{\max}} \rho_s^2(z) (A_i A_j + \frac{1}{8} A'_i A'_j) dz, \quad (16)$$

where  $\rho_m$  is the mass density of the nucleus. In Eq. (16) the primes denote the differentiation with respect to  $z$  and the expansion coefficients,  $A_j$ , are determined from the condition of incompressibility of a compound nucleus, where the time derivative of its volume must vanish.  $A_j(z, q)$  can be given as

$$A_j(z, \mathbf{q}) = -\frac{1}{\rho_s^2(z)} \frac{\partial}{\partial q_j} \int_z^{z_{\max}} \rho_s^2(z') dz'. \quad (17)$$

During a random walk along the trajectory in the collective coordinate space, the total excitation energy of nucleus can be determined by conservation of energy:

$$E^* = E_{\text{int}}(t) + E_{\text{coll}}(\mathbf{q}, \mathbf{p}) + V(\mathbf{q}, I, K, T) + E_{\text{evap}}(t), \quad (18)$$

where  $E_{\text{coll}} = 0.5 \mu_{ij}(\mathbf{q}) p_i p_j$  is the kinetic energy of the nucleus,  $E_{\text{int}}$  is the intrinsic excitation energy of the nucleus,  $E_{\text{evap}}(t)$  is the energy carried away by evaporated particles by time  $t$  and  $V(\mathbf{q}, I, K, T)$  is the potential energy of the compound nucleus.

In the present calculations, the total kinetic energy  $E_k$  of the fission fragments is calculated as the sum of the nuclear attractive energy  $V_n$  of the nascent fragments, the Coulomb repulsion energy  $V_C$  of the fragments, and the kinetic energy  $E_{ps}$ , of their relative motion, all of the terms being calculated at the scission point. Therefore, if the trajectory reaches the scission point the trajectory is treated as a fission event and the mass numbers and total kinetic energy of two fission fragments could be obtained. The mean value of the total kinetic

energy at the scission point can be defined as follows:

$$\langle E_k \rangle = \langle V_C \rangle + \langle V_n \rangle + \langle E_{ps} \rangle. \quad (19)$$

Furthermore, the mass distributions of fission fragments can be calculated by the distribution of  $Y(E_k, M)$ . The fragment masses are calculated by the formulas

$$M_L = \frac{A \int_{z_N}^{z_{\max}} \rho_s^2(z, \mathbf{q}_{sc}) dz}{\int_{z_{\min}}^{z_{\max}} \rho_s^2(z, \mathbf{q}_{sc}) dz},$$

$$M_R = \frac{A \int_{z_{\min}}^{z_N} \rho_s^2(z, \mathbf{q}_{sc}) dz}{\int_{z_{\min}}^{z_{\max}} \rho_s^2(z, \mathbf{q}_{sc}) dz}, \quad (20)$$

where  $A$  is the mass of the nucleus,  $M_L$  and  $M_R$  are the mass of the left and right fission fragment,  $\mathbf{q}_{sc}$  is the scission configuration of the nucleus,  $z_{\min}$  and  $z_{\max}$  are the left and right ends of the nuclear surface, and  $z_N$  is the position of the neck plane that divides the nucleus into two parts. The mass distributions of fission fragments can be calculated by the following formula:

$$Y(M) = \int Y(E_k, M) dE_k. \quad (21)$$

### III. RESULTS AND DISCUSSIONS

A stochastic approach based on the 4D Langevin equations has been used to describe the fission process of the excited compound nucleus  $^{240}\text{Pu}$  produced in neutron-induced reactions at incident energies from thermal to 14 MeV. The fission cross section, the total kinetic energy of fission fragments, the mass distribution of fission fragments, the average prompt neutron multiplicity, the average spin of fission fragments, and the mean fission time have been calculated for  $^{240}\text{Pu}$ . In the dynamical calculations the effects of nuclear dissipation on the fission cross section and the neck radius (at which rupture occurs) on the total kinetic energy of fission fragments have been investigated for the fission process of  $^{240}\text{Pu}$ . In the dynamical calculations, nuclear dissipation was generated through the chaos weighted wall-and-window friction formula with a chaoticity coefficient  $\mu(q_1)$ . It should be mentioned that in the present research for simplicity it is assumed that  $\mu(\mathbf{q}) \cong \mu(q_1)$ . Furthermore, in the dynamical calculations it was assumed that the magnitude of chaoticity coefficient is constant, with its magnitude inferred by reproducing experimental data of the fission cross section for  $^{240}\text{Pu}$ , and the results of calculations for both cases were compared with each other. Figure 5 shows the results of calculations for the fission cross section as a function of incident neutron energy calculated for  $^{240}\text{Pu}$  considering different values of chaoticity coefficient. It should be mentioned that the results of calculations for the fission cross section are not sensitive to the value of the neck radius at which rupture occurs. This is because when a compound nucleus descends from its saddle point, the nucleus with high probability reaches the scission point and splits. Therefore, for reproducing experimental data of the fission cross section for  $^{240}\text{Pu}$  it was assumed that the fission occurred at the radius of the neck equal to zero. Then, after determining the appropriate value for the chaoticity coefficient, the exact value of the neck radius in the scission configuration

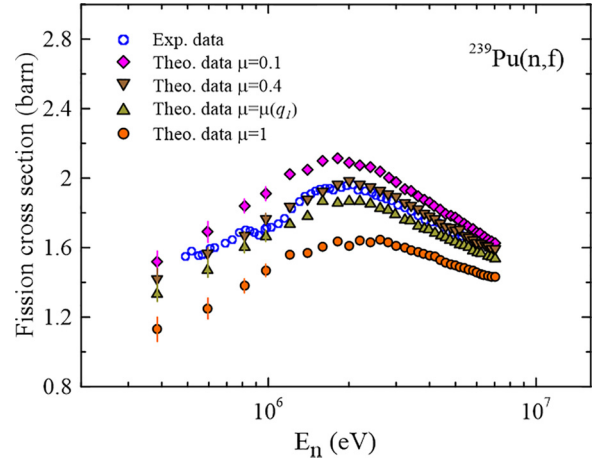


FIG. 5. The fission cross section as a function of incident neutron energy for  $^{240}\text{Pu}$  calculated by using different values of chaoticity coefficient. The lines are error bars. The open circles are experimental data [37].

was determined by reproducing the total kinetic energy for the fission fragments of  $^{240}\text{Pu}$ .

It can be seen from Fig. 5 that the experimental data of the fission cross section for  $^{240}\text{Pu}$  can be satisfactorily reproduced by using  $\mu = 0.4$ . It is also clear from Fig. 5 that the results of calculations at low energies are more sensitive to the magnitude of the  $\mu$  coefficient than at higher energies. It can also be seen from Fig. 5 that, with increasing incident neutron energy, the fission cross section is decreased. It is due to the competition between the fission and the neutron emission of the compound nucleus. When the excitation energy of the compound nucleus is higher than the neutron separation energy, the probability of neutron emission is increased and, with cooling, the compound nucleus probability of fission is decreased. The total kinetic energy of fission fragments is an important fission observables as it reveals further information on the excitation energy distribution of fission fragments for the calculation of prompt fission neutron multiplicities. It should be mentioned that many authors, for the description of the fission process of excited compound nuclei, assumed that the fission occurred in a configuration for which the radius of the neck vanishes. However, scission should occur before the nucleus reaches this configuration because of the balance between the Coulomb and nuclear forces during the dynamical descent from the saddle point. For large necks the nucleus is stable against neck rupture, because the repulsive Coulomb force is smaller than the attractive nuclear force. Then, the attractive nuclear force becomes smaller in magnitude than the repulsive Coulomb force and then the neck ruptures at a nonzero radius. It should be noted that the sum of the Coulomb and nuclear interaction energies between the two portions is initially attractive but becomes repulsive when the neck reaches a critical size. It should also be noted that the rupture of the neck at a finite radius plays an important role in the post-scission dynamics of fission. The size of the neck when it ruptures may be estimated for a nucleus by reproducing experimental data of the kinetic energy of

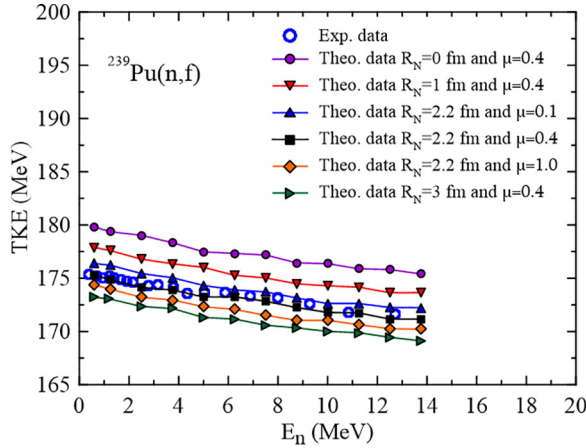


FIG. 6. The total kinetic energy of fission fragments of  $^{240}\text{Pu}$  produced in the  $n + ^{239}\text{Pu}$  reaction at incident energies from thermal to 14 MeV calculated by using different values of neck radius at which scission occurs. The calculated values are connected by solid lines to guide the eye. The open circles are experimental data [38].

fission fragments. Figure 6 shows the results of the total kinetic energy of fission fragments as a function of incident neutron energy calculated for  $^{240}\text{Pu}$  by using different values of neck radius and by using  $\mu = 0.4$ . It is clear from Fig. 6 that the kinetic energy of the fission fragments calculated by using a nonzero radius decreases relative to that calculated for scission occurring at zero neck radius. In general, the kinetic energy of the fission fragments is quite sensitive to the nuclear shapes at the scission point. It is also clear from Fig. 6 how incident neutron energy influences on the values of the average total kinetic energies of fission fragments of  $^{240}\text{Pu}$ . It can also be seen from Fig. 6 that the results of calculations are very sensitive to neck radius. It is clear from Fig. 6 that the experimental data on the kinetic energy of the fission fragments for  $^{240}\text{Pu}$  can be satisfactorily reproduced by using the magnitude of the neck radius at which scission occurs equal to 2.2 fm. In Fig. 6, for a more accurate comparison, the results of calculations were compared with the results calculated with  $R_n = 2.2$  fm and  $\mu = 0.1$  and 1. It is also clear from Fig. 6 that the average total kinetic energies of fission fragments of  $^{240}\text{Pu}$  decrease with increasing projectile energy.

It should be mentioned that the results of calculations for the total kinetic energy of fission fragments are also sensitive to nuclear viscosity. Figure 7 shows the results of calculations for the total kinetic energy of fission fragments of  $^{240}\text{Pu}$  calculated by using different values of the chaoticity coefficient  $\mu$  and by using the value of neck radius at which scission occurs equal to 2.2 fm. In Fig. 7, for a more accurate comparison, the results of calculations were compared with the results of calculations calculated with  $R_n = 0, 1,$  and 3 fm and  $\mu = 0.4$ . It can be seen from Fig. 7 that the results of calculations calculated for the total kinetic energy of fission fragments for  $^{240}\text{Pu}$  decreased with increasing viscosity. This decrease arises from a combination of two effects. With increasing viscosity the system arrives in the scission configuration with less kinetic energy, and also with increasing viscosity the scission configuration is more elongated, which this decreases

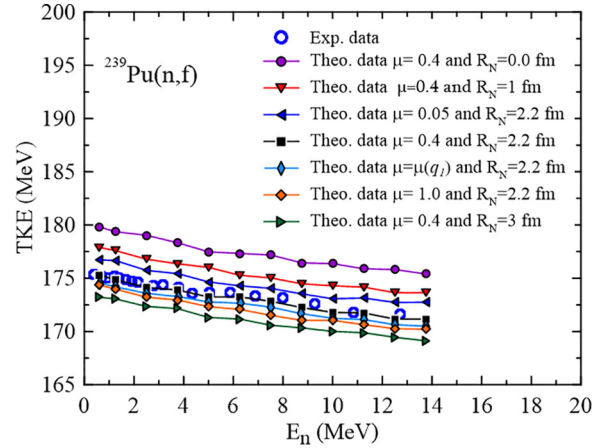


FIG. 7. Same as Fig. 6, but the total kinetic energy of fission fragments of  $^{240}\text{Pu}$  calculated by using different values of the chaoticity coefficient  $\mu$  and by using the value of neck radius at which scission occurs equal to 2.2 fm. The calculated values are connected by solid lines to guide the eye. The open circles are experimental data [38].

the Coulomb interaction energy and hence decreases the total kinetic energy of fission fragments.

In the present investigation, the mass yield distribution of fission fragments and the average prompt neutron multiplicity have also been calculated for the compound nucleus  $^{240}\text{Pu}$  in order to evaluate the extracted values of the chaoticity coefficient  $\mu = 0.4$  and the neck radius 2.2 fm. Figures 8–10 show the results of calculations for the mass yield distribution of fission fragments and the average prompt neutron multiplicity for  $^{240}\text{Pu}$ .

It should be mentioned that the kinetic energy of thermal neutrons was assumed to be zero, so the excitation energy of the  $^{240}\text{Pu}$  nucleus considered equals 6.53 MeV.

It can be seen from Fig. 8 that there is a good agreement between the calculated results and the experimental data for

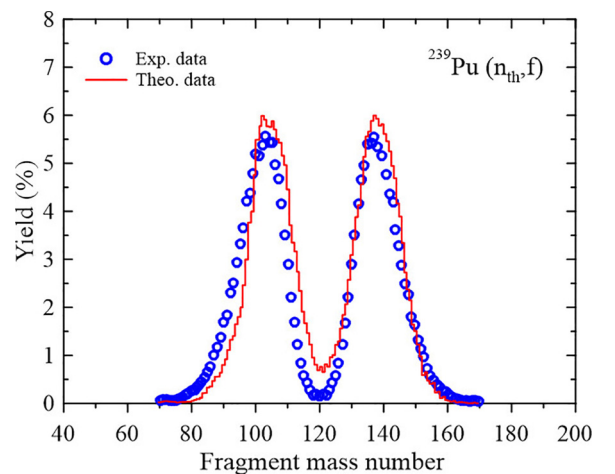


FIG. 8. The results of the mass yield distribution of fission fragments of  $^{240}\text{Pu}$  with the excitation energy equal to 6.53 MeV produced in reactions with thermal neutrons. The open circles are experimental data [39].

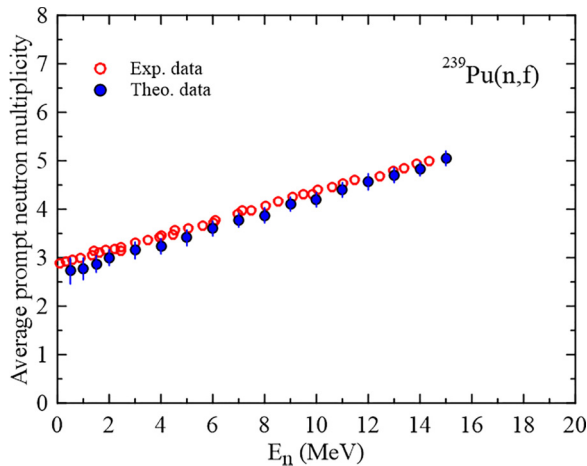


FIG. 9. The average prompt neutron multiplicity as a function of incident neutron energy for  $^{240}\text{Pu}$  produced in the  $n + ^{239}\text{Pu}$  reaction calculated by using the value of chaoticity coefficient  $\mu = 0.4$  and the value of neck radius at which scission occurs equal to 2.2 fm. The lines are error bars. The open circles are experimental data [40].

both symmetric and asymmetric fission regions. Furthermore, most of the fission events are distributed around the heavy fragment mass  $A \approx 135$ , where the heavy fragment is close to spherical shape due to the shell effects around the shell closure  $Z = 50$  and  $N = 82$ . Furthermore, it can be seen from Fig. 8 that the positions and widths of the peaks are also reproduced with high accuracy. It can also be seen from Fig. 10 that the prompt neutron distribution has the typical sawtooth shape. The physical origin of the sawtooth shape in neutron multiplicity is due to the mean number of fission neutrons emitted being a function of the fission fragment mass split. This dependence on the fragment mass split is predominantly caused by nuclear shell effects and exhibits the well-known sawtooth distributions. It is also clear from Figs. 8–10 that

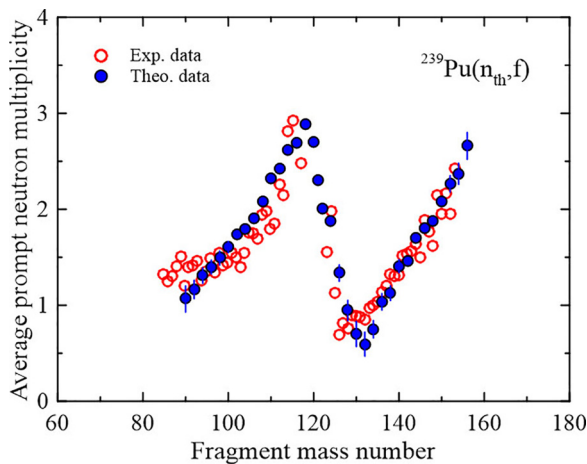


FIG. 10. Same as Fig. 9 but for the average prompt neutron multiplicity as a function of fission fragment mass of  $^{240}\text{Pu}$  with the excitation energy equal to 6.53 MeV produced in reactions with thermal neutrons. The lines are error bar. The open circles are experimental data [39].

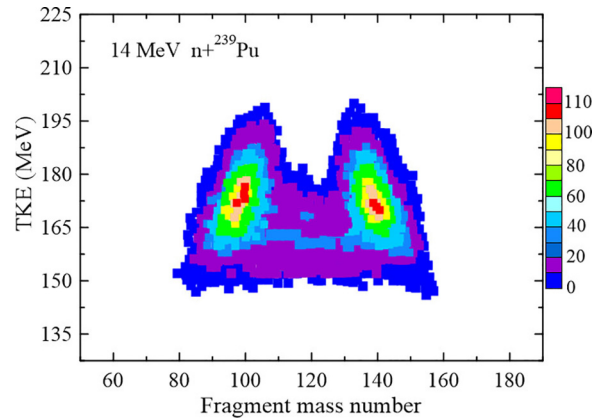


FIG. 11. The results of mass energy correlation of fission fragments for  $^{240}\text{Pu}$  produced in 14 MeV  $n + ^{239}\text{Pu}$  fission. The color scale on the right side of the figure is the yield of the fission fragments.

the results of calculations for the mass yield distribution of fission fragments and the average prompt neutron multiplicity for  $^{240}\text{Pu}$  quantitatively agree with the experimental data by using the values of the chaoticity coefficient equal to  $\mu = 0.4$  and the neck radius in the scission configuration equal to 2.2 fm. In the present investigation, the mass energy correlations of the fission fragments have been calculated in 14 MeV  $n + ^{239}\text{Pu}$  fission. Figure 11 shows the results of mass energy correlation of fission fragments for  $^{240}\text{Pu}$  produced in 14 MeV  $n + ^{239}\text{Pu}$  fission.

In the present investigation, the average spin of fission fragments as a function of mass number was calculated for the compound nucleus  $^{240}\text{Pu}$  produced in thermal-neutron-induced reactions. Figure 12 shows the results of the average spin of fission fragments for the compound nucleus  $^{240}\text{Pu}$ .

It can be seen from Fig. 12 that the average spin of fission fragments is strongly mass dependent and has a sawtooth shape. These results are similar the results obtained in Ref. [41].

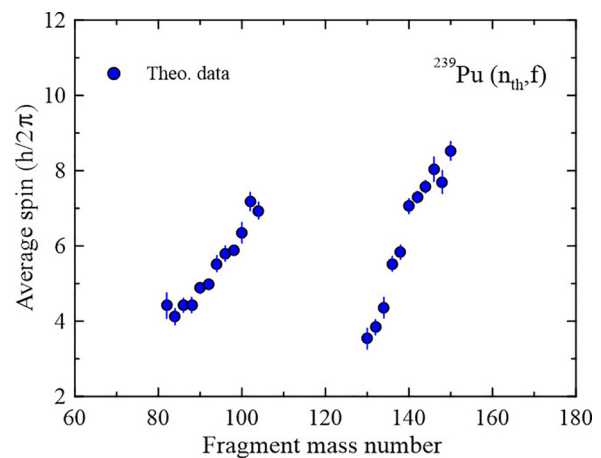


FIG. 12. The average spin of fission fragments as a function of fission fragment mass for  $^{240}\text{Pu}$  produced in thermal-neutron-induced reactions. The lines are error bars.

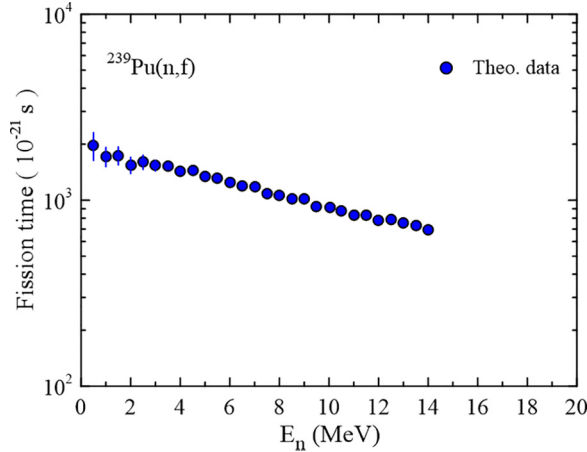


FIG. 13. The results of the mean fission time as a function of incident neutron energy for  $^{240}\text{Pu}$  produced in the  $n + ^{239}\text{Pu}$  reaction. The lines are error bar.

Finally, in the present research the mean fission time has been calculated for the excited compound nucleus  $^{240}\text{Pu}$ . Figure 13 shows the results of the mean fission time as a function of incident neutron energy for  $^{240}\text{Pu}$  produced in the  $n + ^{239}\text{Pu}$  reaction. It can be seen from Fig. 13 that the mean fission time decreases rapidly with increasing incident neutron energy.

It should be mentioned that Nadochay *et al.* in Ref. [12] used the 4D dynamical model to calculate different experimental data for the excited compound nuclei  $^{199}\text{Pb}$  and  $^{248}\text{Cf}$  produced in heavy-ion-induced reactions. In their calculations in the Langevin equations, they used the modified version of the one-body dissipation mechanism, with different constant reduction coefficients  $k_s$  and also the coordinate-dependent reduction coefficient  $k_s(\mathbf{q})$  calculated on the basis of the chaos-weighted wall formula. The results of their calculations showed that it is not possible to detect some “universal”  $k_s$  value, which could provide good reproduction of all experimental observables for heavy and light fissioning nuclei. They showed that most of the experimental observables could be reproduced in 4D calculations with  $k_s$  close to one for the  $^{199}\text{Pb}$  compound nucleus. Furthermore, they showed that for the heavier compound nucleus  $^{248}\text{Cf}$  the variance of the kinetic energy distribution could be reproduced with  $k_s$  around 0.5 or  $k_s(\mathbf{q})$  obtained from the chaos-weighted wall formula. Some other works of Nadochay *et al.* about the viscosity of nuclear matter are Refs. [42–49].

It should also be mentioned that the results extracted in the present research for the relationship between the neck radius and the TKE are similar to those of the previous study. The present study shows that the change in neck radius at scission from 1 to 2.2 fm for  $^{240}\text{Pu}$  leads to the change in TKE from 177.9 to 175.3 MeV, the difference being 2.6 MeV. Sierk in Ref. [50] studied the relationship between the neck radius and the TKE and found that the change in neck radius at scission from 1 to 2 fm for  $^{236}\text{U}$  leads to the change in TKE from 173.6 to 170.9 MeV, whose difference is 2.7 MeV. Furthermore, the

value of neck radius that is inferred in the present research is also consistent with the work of Davies *et al.* in Ref. [51]. Davies *et al.* in Ref. [51] introduced a degree of freedom to describe the rupture of the neck in nuclear fission and calculated the point at which the neck ruptures as the nucleus descends dynamically from its fission saddle point. This was done by dividing the system into two portions at its minimum neck radius and calculating the force required to separate the two portions while keeping their shapes fixed. This force was obtained by differentiating with respect to separation the sum of the Coulomb and nuclear interaction energies between the two portions. They calculated this force along dynamical paths leading from the fission saddle point for nuclei throughout the periodic table. The force is initially attractive but becomes repulsive when the neck reaches a critical size. They showed that for actinide nuclei the neck radius at which rupture occurs is about 2 fm.

#### IV. CONCLUSIONS

In the framework of the 4D Langevin equations, the fission process of the excited compound nucleus  $^{240}\text{Pu}$ , produced in neutron-induced reactions at incident energies from thermal to 14 MeV, has been described. The fission cross section, the total kinetic energy of fission fragments, the mass distribution of fission fragments, the average prompt neutron multiplicity, the average spin of fission fragments, and the mean fission time have been calculated for  $^{240}\text{Pu}$ . In the dynamical calculations the effects of nuclear dissipation and the neck radius at which rupture occurs on the fission cross section and the total kinetic energy of fission fragments of  $^{240}\text{Pu}$  were investigated. In the dynamical calculations, nuclear dissipation was generated through the chaos weighted wall-and-window friction formula with a chaoticity coefficient  $\mu(q_1)$ . Furthermore, in the dynamical calculations it was assumed that the magnitude of the chaoticity coefficient is constant and its magnitude was inferred by reproducing experimental data of the fission cross section for  $^{240}\text{Pu}$ , and the results of calculations for both cases were compared with each other. It was shown that the results of calculations for the fission cross section are in good agreement with the experimental data by using the magnitude of the chaoticity coefficient  $\mu = 0.4$ . Furthermore, by reproducing experimental data on the total kinetic energy of fission fragments, the magnitude of the neck radius at which rupture occurs was inferred. It was shown that the results of calculations for the total kinetic energy of fission fragments of  $^{240}\text{Pu}$  are in good agreement with the experimental data by using the magnitude of the radius in the scission configuration equal to 2.2 fm. In the present research, the mass distribution of fission fragments and the average prompt neutron multiplicity were also calculated for  $^{240}\text{Pu}$  in order to evaluate the extracted values of the chaoticity coefficient  $\mu$  and the neck radius in the scission configuration. It was shown that the results of calculations for the mass distribution of fission fragments and the average prompt neutron multiplicity are in good agreement with the experimental data by using these appropriate values for the chaoticity coefficient and the radius



of the scission configuration. Finally, in the present research, the average spin of fission fragments and the mean fission time were calculated for  $^{240}\text{Pu}$ . It was shown that the average spin of fission fragments is strongly mass dependent and has a sawtooth shape, and also the mean fission time decreases rapidly with increasing incident neutron energy.

## ACKNOWLEDGMENTS

The author thanks the anonymous referee for comments and suggestions, which led to a significantly improved version of this paper. Support of the Research Committee of the Persian Gulf University is greatly acknowledged.

- 
- [1] C. Ishizuka, X. Zhang, M. D. Usang, F. A. Ivanyuk, and S. Chiba, *Phys. Rev. C* **101**, 011601(R) (2020).
- [2] M. D. Usang, F. A. Ivanyuk, C. Ishizuka, and S. Chiba, *Sci. Rep.* **9**, 1525 (2019).
- [3] V. Y. Denisov and I. Y. Sedykh, *Eur. Phys. J. A* **57**, 129 (2021).
- [4] J. Tian, N. Wang, and W. Ye, *Phys. Rev. C* **95**, 041601(R) (2017).
- [5] H. Eslamizadeh, *Int. J. Mod. Phys. E* **24**, 1550052 (2015).
- [6] H. Eslamizadeh and H. Raanaei, *Ann. Nucl. Energy* **51**, 252 (2013).
- [7] L. L. Liu, X. Z. Wu, Y. J. Chen, C. W. Shen, Z. G. Ge, and Z. X. Li, *Phys. Rev. C* **105**, 034614 (2022).
- [8] H. Eslamizadeh, *Phys. Rev. C* **94**, 044610 (2016).
- [9] H. Eslamizadeh, *J. Phys. G: Nucl. Part. Phys.* **40**, 095102 (2013).
- [10] M. Shareef, E. Prasad, A. Jhingan, N. Saneesh, S. Pal *et al.*, *Phys. Rev. C* **107**, 054619 (2023).
- [11] H. Eslamizadeh and H. Razazzadeh, *Phys. Lett. B* **777**, 265 (2018).
- [12] P. N. Nadtochy, E. G. Ryabov, A. V. Cheredov, and G. D. Adeev, *Eur. Phys. J. A* **52**, 308 (2016).
- [13] N. Kumari, A. Deep, and R. Kharab, *Phys. Rev. C* **105**, 014628 (2022).
- [14] H. Eslamizadeh and E. Ahadi, *Phys. Rev. C* **96**, 034621 (2017).
- [15] H. Eslamizadeh, *Pramana J. Phys.* **78**, 231 (2012).
- [16] J. P. Lestone, *Phys. Rev. C* **59**, 1540 (1999).
- [17] A. V. Karpov, P. N. Nadtochy, D. V. Vanin, and G. D. Adeev, *Phys. Rev. C* **63**, 054610 (2001).
- [18] A. V. Ignatyuk, G. N. Smirenkin, and A. S. Tishin, *Sov. J. Nucl. Phys.* **21**, 255 (1975).
- [19] J. Maruhn and W. Greiner, *Z. Phys.* **251**, 431 (1972).
- [20] P. Fröbrich and I. I. Gontchar, *Phys. Rep.* **292**, 131 (1998).
- [21] S. G. McCalla and J. P. Lestone, *Phys. Rev. Lett.* **101**, 032702 (2008).
- [22] T. Døssing and J. Randrup, *Nucl. Phys. A.* **433**, 215 (1985).
- [23] J. Randrup, *Nucl. Phys. A.* **383**, 468 (1982).
- [24] K. T. R. Davies and J. R. Nix, *Phys. Rev. C* **14**, 1977 (1976).
- [25] J. P. Lestone and S. G. McCalla, *Phys. Rev. C* **79**, 044611 (2009).
- [26] H. J. Krappe, J. R. Nix, and A. J. Sierk, *Phys. Rev. C* **20**, 992 (1979).
- [27] A. J. Sierk, *Phys. Rev. C* **33**, 2039 (1986).
- [28] V. M. Strutinsky, *Nucl. Phys. A.* **95**, 420 (1967).
- [29] S. G. Nilsson, C. F. Tsang, A. Sobieczewski, Z. Szymański, S. Wycech, C. Gustafson, I. L. Lamm, P. Möller, and B. Nilsson, *Nucl. Phys. A.* **131**, 1 (1969).
- [30] T. Asano, T. Wada, M. Ohta, T. Ichikawa, S. Yamaji, and H. Nakahara, *J. Nucl. Radiochem. Sci.* **5**, 1 (2004).
- [31] M. Brack, J. Damgaard, A. S. Jensen, H. C. Pauli, V. M. Strutinsky, and C. Y. Wong, *Rev. Mod. Phys.* **44**, 320 (1972).
- [32] V. M. Strutinsky, *Nucl. Phys. A.* **122**, 1 (1968).
- [33] S. Pal and T. Mukhopadhyay, *Phys. Rev. C* **57**, 210 (1998).
- [34] J. Blocki, F. Brut, T. Srokowski, and W. Swiatecki, *Nucl. Phys. A.* **545**, 511 (1992).
- [35] D. V. Vanin, G. I. Kosenko, and G. D. Adeev, *Phys. Rev. C* **59**, 2114 (1999).
- [36] K. T. R. Davies, A. J. Sierk, and J. R. Nix, *Phys. Rev. C* **13**, 2385 (1976).
- [37] F. Tovesson and T. S. Hill, *Nucl. Sci. Eng.* **165**, 224 (2010).
- [38] F. Tovesson, D. Duke, V. Geppert-Kleinrath, B. Manning, D. Mayorov, S. Mosby, and K. Schmitt, *EPJ Web Conf.* **169**, 00024 (2018).
- [39] C. Tsuchiya, Y. Nakagome, H. Yamana, H. Moriyama, K. Nishio, I. Kanno, K. Shin, and I. Kimura, *J. Nucl. Sci. Technol.* **37**, 941 (2000).
- [40] V. V. Malinovskij, V. G. Vorob'eva, and B. D. Kuz'minov, IAEA Report No. INDC (CCP)-239, 1985 (unpublished).
- [41] J. N. Wilson *et al.*, *Nature (London)* **590**, 566 (2021).
- [42] P. N. Nadtochy, G. D. Adeev, and A. V. Karpov, *Phys. Rev. C* **65**, 064615 (2002).
- [43] P. N. Nadtochy, E. G. Ryabov, A. E. Gegechkori, Yu. A. Anischenko, and G. D. Adeev, *Phys. Rev. C* **89**, 014616 (2014).
- [44] P. N. Nadtochy, E. G. Ryabov, and G. D. Adeev, *J. Phys. G: Nucl. Part. Phys.* **42**, 045107 (2015).
- [45] P. N. Nadtochy, E. G. Ryabov, A. E. Gegechkori, Yu. A. Anischenko, and G. D. Adeev, *Phys. Rev. C* **85**, 064619 (2012).
- [46] P. N. Nadtochy, A. V. Karpov, and G. D. Adeev, *Phys. At. Nucl.* **65**, 832 (2002).
- [47] D. V. Vanin, P. N. Nadtochy, G. I. Kosenko, and G. D. Adeev, *Phys. At. Nucl.* **63**, 1957 (2000).
- [48] P. N. Nadtochy, E. G. Ryabov, A. E. Gegechkori, Yu. A. Anischenko, and G. D. Adeev, *EPJ Web Conf.* **62**, 07001 (2013).
- [49] P. N. Nadtochy, E. Vardaci, A. Di Nitto, A. Brondi, G. La Rana, R. Moro, M. Cinausero, G. Prete, N. Gelli, and F. Lucarelli, *Phys. Lett. B* **685**, 258 (2010).
- [50] A. J. Sierk, *Phys. Rev. C* **96**, 034603 (2017).
- [51] K. T. R. Davies, R. A. Managan, J. R. Nix, and A. J. Sierk, *Phys. Rev. C* **16**, 1890 (1977).